AJNR

MR of the cauda equina.

A Monajati, W S Wayne, W Rauschning and S E Ekholm

AJNR Am J Neuroradiol 1987, 8 (5) 893-900
http://www.ajnr.org/content/8/5/893

MR of the Cauda Equina

Ahmad Monajati[1]
William S. Wayne[2]
Wolfgang Rauschning[3]
Sven Erling Ekholm[4]

To define the anatomy of the cauda equina nerve roots by MR imaging, the lower spine of 14 normal volunteers was imaged using a high-field surface-coil technique. A total of 56 sagittal and 56 axial MR sections (eight selected slices from each case) were correlated with undistorted anatomic sections from cadaver spine specimens, and the visualization of the nerve roots was assessed. In addition, MR images of three patients with infiltrating or seeding tumors affecting the cauda equina were analyzed. Seventy-eight percent of the MR sections from normal cases clearly showed the anatomy of the cauda equina nerve roots. The nerve roots were fairly shown in 17% of the sections; and false findings (presumably caused by CSF pulsation) were observed in the remaining 5%. Coronal imaging provided excellent anatomic views of the nerve roots within the intervertebral foramina. Morphologic alterations in the pathologic cases were correctly shown when both T1- and T2-weighted imaging were used.

In conclusion, MR proved efficient in viewing the cauda equina region.

The effectiveness of MR in viewing the normal and pathologic spinal cord has been well documented [1–6]. Limited resolution in discriminating subarachnoid nerve roots from the surrounding CSF, however, has not permitted adequate display of the cauda equina [1, 2]. High-field surface-coil MR techniques have been shown to augment the image contrast and spatial resolution [7–9]. The aim of the present study is to better define the normal morphologic anatomy of the cauda equina as perceived by high-field surface-coil MR imaging and to illustrate pathologic morphology in three cases of infiltrating neoplastic disease in this region.

Materials and Methods

Fourteen healthy volunteers (nine men, five women, 24–48 years old) had MR of the lower spine. MR scans were obtained on a 1.5-T superconducting magnet (GE Signa) unit. A surface coil measuring 7 × 12.5 in. diameter was used. The data matrix was 256 × 256, which, with a field of view of 24 cm in the sagittal plane, yielded a pixel size of 0.94 × 0.94 mm. In the axial plane, a field of view of 20 cm was used, yielding a pixel size of 0.78 × 0.78 mm. Four excitations were used with two averages. A single spin-echo sequence with repetition time (TR) = 500 msec and echo time (TE) = 25 msec, and a multiecho sequence of TR = 2000 msec with variable TEs of 25 and 100 msec were used. These MR sequences provided T1- and T2-weighted images.

Contiguous 5-mm-thick images were obtained both in sagittal and axial planes in all cases. For each case the imaging was completed in two sets: the first with the surface coil centered on the thoracic-lumbar region (Fig. 1A) and the second with the surface coil centered approximately on the middle of the lumbar region (Fig. 1C). In each set an axial localizing image (TR 400/TE 25 msec, 10-mm slice thickness, one excitation, 1-min scan time) was first used to localize the sagittal sections. From a point 20 or 25 mm (depending on the transverse vertebral thickness) lateral to and right of the center of the spinal canal, to an equidistant point on the left side, the spine was scanned using contiguous 5-mm-thick slices. This allowed symmetrical sectioning of the right and left intervertebral foramina and cutting one slice through the midline of the spinal canal. A sagittal scout view (a midline 10-mm-thick

Received November 18, 1986; accepted after revision March 5, 1987.

[1] Department of Diagnostic Radiology/Nuclear Imaging, University of Rochester School of Medicine and Dentistry, and Rochester General Hospital, 1425 Portland Ave., Rochester, NY 14621. Address reprint requests to A. Monajati.

[2] Department of Radiology, University of Rochester School of Medicine and Dentistry, Rochester, NY 14642.

[3] Department of Orthopedic Surgery, University Hospital, S-75, 185 Uppsala, Sweden.

[4] Department of Radiology, Section of Neuroradiology, University of Rochester School of Medicine and Dentistry, Rochester, NY 14642.

AJNR 8:893–900, September/October 1987
0195–6108/87/0805–0893

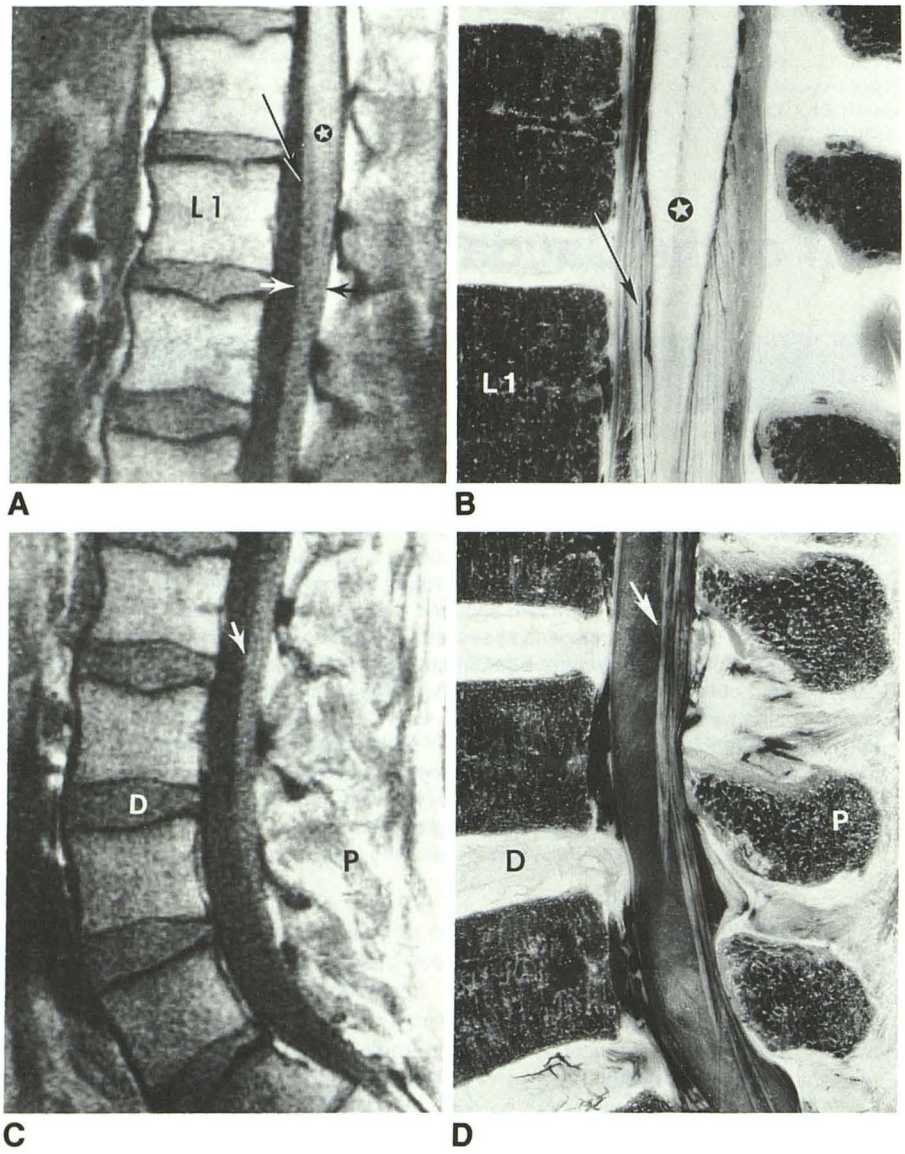

Fig. 1.—Mid-sagittal view of conus medullaris and cauda equina nerve root bundles.

***A* and *C*, MR images from normal volunteer (T1-weighted, spin-echo, TR 500/TE 25 msec).**

***B* and *D*, Cadaver anatomic sections through midline sagittal plane of thoracic-lumbar and lumbar regions. Good delineation of conus (*asterisk*) and nerve root bundles (*short arrows*) are shown by MR. Interface between ventral nerve root bundle (*long arrow*) and conus is clearly seen. Note that silhouette of nerve root bundles appears as a uniform intermediate intensity located in posterior aspect of dural sac. D = intervertebral disk; p = posterior spinal process.**

image obtained with a larger field of view of 32 or 40 cm, a body coil, and 1 min scan time) was used to identify the level of the lumbar vertebrae in reference to the sacrum. Axial imaging was performed in each set by using the midline sagittal section as a localizing image. Contiguous 5-mm-thick sections were then obtained from the middle of T12 to the middle of L2 vertebral body in the first set and from the middle of L2 to the top of L4 in the second set.

We selected the following eight image sections from each case to study. In the sagittal plane four slices were chosen: the midline, one at 5 and one at 10 mm off midline, and one through the level of the neural foramina. The selected axial images included sections through the T12–L1 disk space, the mid portions of the L1 and L2 vertebral bodies, and the L3–L4 disk space (four slices).

Undistorted cadaver anatomic sections of approximately the same topography as the MR images were obtained for correlation. These were prepared from spinal specimens of postmortem patients using cryomicrotomy technique [10]. With regard to anatomy of the cauda equina, the MR images were compared with the photographs of the matching anatomic sections. The visualization of the nerve root bundles with respect to anatomic correlation was assessed by visual inspection using four gradings (Table 1). A total of 56 sagittal and 56 axial sections (14 cases, eight slices each) were evaluated (Figs. 1–4). Coronal imaging with a higher-resolution technique (see Fig. 8) was performed in a few cases but were not considered in the tabulation because spine curvature made it technically difficult to consistently produce MR sections comparable to cadaver anatomic sections.

MR images of three cases with proven pathology were reviewed. These images had been obtained in sagittal and axial planes using the same MR parameters as in the volunteer cases above except that two excitations (one average) were used.

Case 1

A 35-year-old man was admitted for evaluation of back pain radiating into the buttocks of 1 week duration. He had no bowel or

bladder dysfunction. Physical examination revealed intact cranial nerves but decreased muscle strength and abnormal deep tendon reflexes of the left leg. A lumbar myelogram showed an intradural block at the L2 level. Lumbar puncture showed a CSF protein concentration of 420 mg/dl. MR imaging is shown in Figure 5.

TABLE 1: Assessment of MR Visualization of the Cauda Equina Nerve Roots with Regard to Anatomic Correlation (14 cases, 112 image sections)

Gradings (Visual Inspection)	Sagittal Sections	Axial Sections	Total No.	(%)
Excellent	17	0	17	(15)
Adequate	28	42	70	(63)
Undecided	5	14	19	(17)
False	6	0	6	(5)
Total	56	56	112	100

Note.—Excellent = nerve bundles were clearly outlined on MR scan and almost completely matched their anatomic counterparts; adequate = nerve bundles were adequately outlined and for the most part matched their anatomic counterparts; undecided = nerve-roots image was not clear enough to match its anatomic counterpart; false = findings on MR images (partially or totally) could not be anatomically explained.

Surgery revealed an intradural multinodular lesion in the upper lumbar area attached to the nerve roots and the filum, extending from the T12–L1 level to the middle of L2. The lesion was subtotally resected. Pathologic examination showed a myxopapillary ependymoma. The patient was subsequently referred for radiation therapy of the lumbar region.

Case 2

A 25-year-old man was admitted for radiologic investigation of complaint of back and leg pain. He had been in good health except that in the last 2 years he had noted some discomfort in his low back. About 4 months before admission he noticed that the back pain was radiating to the upper part of his left leg. This was initially thought to be due to disk disease and was treated with conservative measures. The pain continued to increase and he was referred for further evaluation. Physical examination on admission did not reveal motor or sensory deficit and the tendon reflexes were normal. Plain radiography of the spine was normal, but CT showed soft-tissue density in the sacral canal. Conventional myelography revealed blocks in the upper and lower lumbar regions. CT after myelography showed intradural masses. The CSF collected at the time of myelography revealed markedly elevated protein content (4000 mg/dl). MR imaging is shown in Figure 6.

At surgery (laminectomy at two locations, one in the thoracolumbar

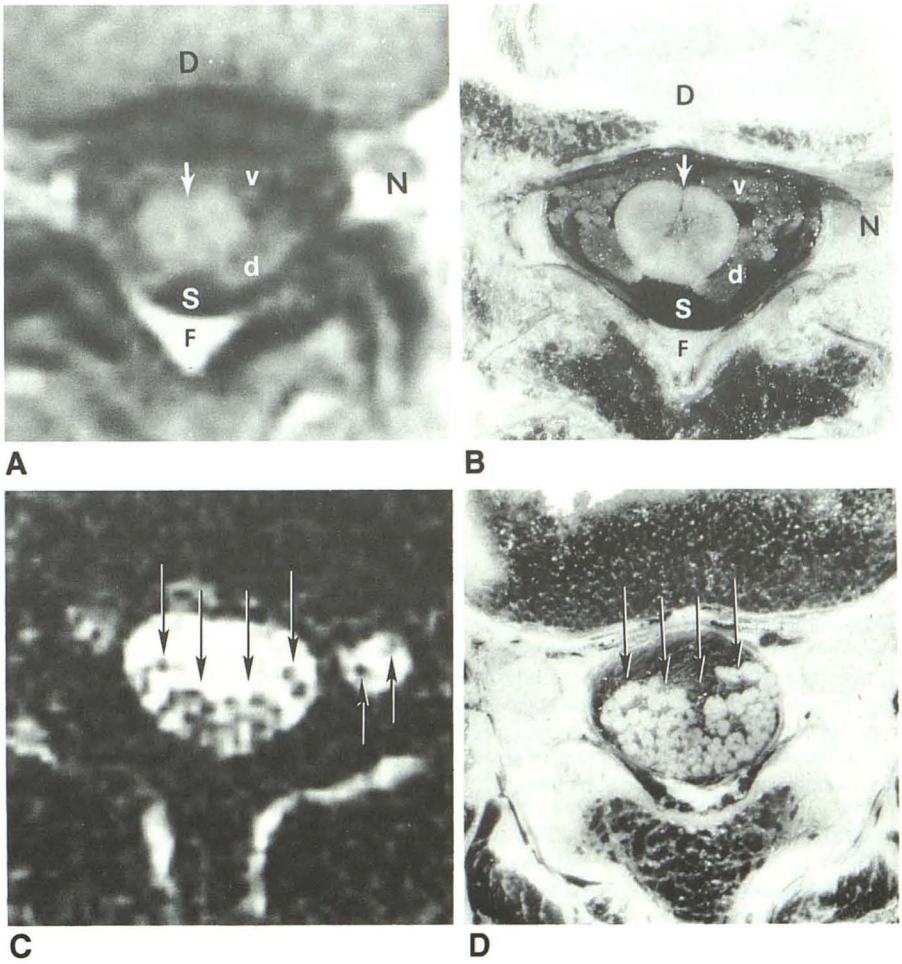

Fig. 2.—Axial view of conus medullaris and cauda equina nerve roots.

***A*, MR image from normal volunteer (T1-weighted spin-echo, TR 500/TE 25 msec).**

***B*, Cadaver anatomic section through T12–L1 space. Conus (*arrow*, pointing to anterior median fissure), nerve root bundles (v = ventrolateral, d = dorsolateral), and surrounding CSF (S) are adequately shown by MR. D = intervertebral disk; N = neural foramen; F = epidural fat.**

***C*, MR image of normal volunteer (T2-weighted, spin-echo, TR 2000/TE 100 msec).**

***D*, Cadaver anatomic section through L3–L4 space. Nerve roots within thecal sac (*downward arrows*) individually or in clusters are well visualized by MR. They are predominantly located in posterior aspect of dural sac and almost symmetrically spread. Note individual nerves with cross section of sleeve (*upward arrows*) before forming ganglion.**

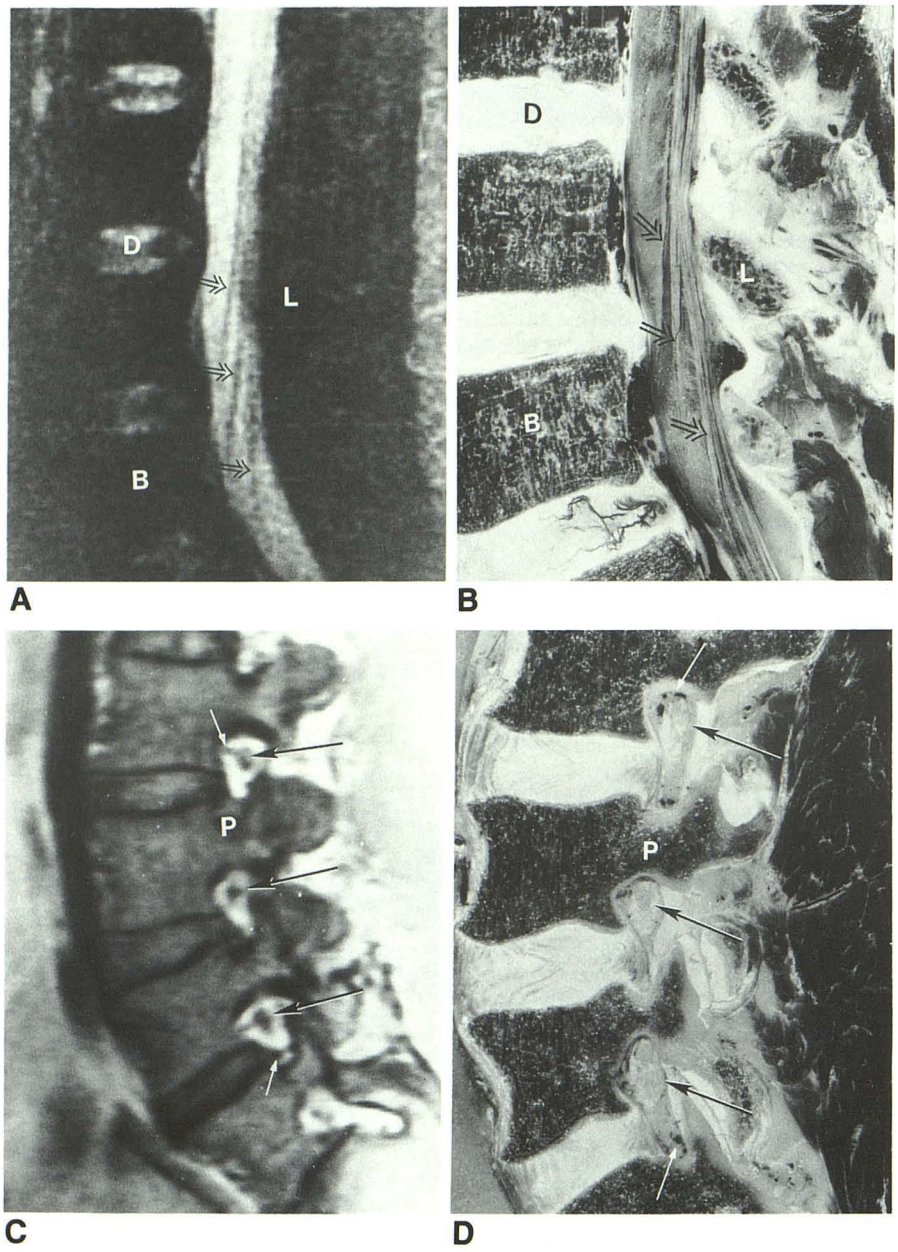

Fig. 3.—Paramidline sagittal views of nerve roots of cauda equina.

***A*, MR image from normal volunteer (T2-weighted, spin-echo, TR 2000/TE 100 msec).**

***B*, Cadaver anatomic section through lumbar spine at about 5 mm off midline. Individual nerve roots (*arrows*) are adequately visualized by MR. Note their smooth, thin, linear appearance. D = intervertebral disk; B = vertebral body; L = lamina.**

***C*, MR image of normal volunteer (T1-weighted, spin-echo TR 500/TE 25 msec).**

***D*, Cadaver anatomic section through lumbar spine at level of neural foramina. Nerve-root-sleeve units (*large arrows*) are seen in clear contrast to surrounding high-intensity fat. They are situated immediately beneath pedicles (P). *Small arrows* point to veins.**

region extending from T10 to L3 and the other in the sacrum), gray-pinkish masses were evident, involving the conus region and the nerves of cauda equina. Tumor masses identical to that of the upper lumbar section were noted to be partially filling the thecal cul de sac and, in some parts, adhering to the adjacent dura. Piecemeal, partial removal of the tumors was done in both regions. Histological examination revealed a myxopapillary type of ependymoma and the patient was subsequently put on radiation therapy.

Case 3

A 45-year-old man with documented malignant melanoma on his shoulder was admitted for evaluation of a 2-month history of right back and upper leg pain. He had no bowel or bladder dysfunction and the cranial nerves were intact. However, physical examination revealed an absent knee jerk on the right, absent ankle jerks bilaterally, and downgoing toes. Sensory tests showed anesthesia in the right calf and decreased vibratory discrimination bilaterally in the toes.

Chest radiography showed multiple pulmonary nodules consistent with metastases. Lumbar spine CT showed soft-tissue density within the canal. Head CT revealed three small enhancing lesions with surrounding edema involving cerebral parenchyma compatible with metastasis. MR imaging of the lumbar spine is shown in Figure 7. Examination of the lumbar CSF revealed protein of 123 mg/dl and malignant melanoma cells. Radiation therapy was instituted to the cauda equina to control his pain.

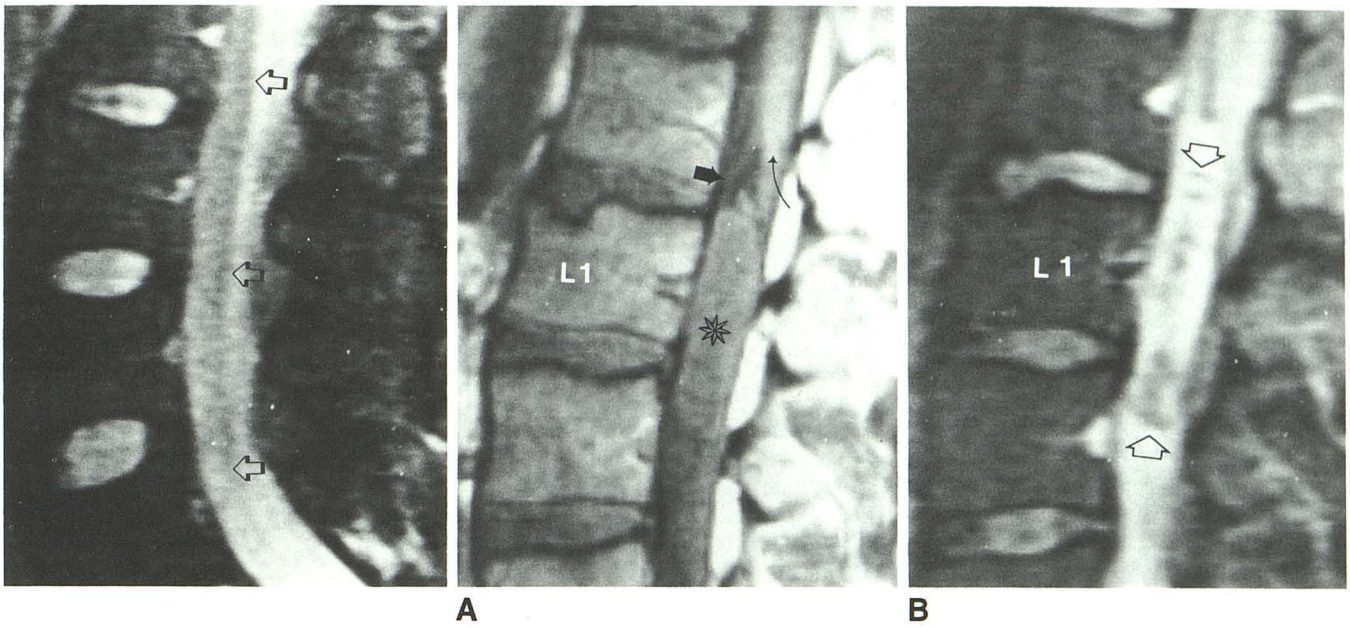

Fig. 4.—Artifact (presumably due to CSF pulsation). Mid-sagittal T2-weighted MR image (spin-echo, TR 2000/TE 100 msec) of lumbar spine shows a longitudinal zone of low intensity (*arrows*) within high-intensity CSF; it does not correlate with any anatomic structures.

Fig. 5.—Case 1. Ependymoma involving region of cauda equina.
***A*, Mid-sagittal T1-weighted (spin-echo, TR 500/TE 25 msec) MR image shows a lesion of intermediate intensity (*asterisk*) displacing ventral nerve root bundle forward (*straight arrow*) and conus backward (*curved arrow*). Note irregular contour of superior aspect of lesion.**
***B*, Mid-sagittal T2-weighted (spin-echo, TR 2000/TE 100 msec) MR image shows lesion to have a multinodular appearance (*arrows*) correlating with surgical finding.**

Results and Discussion

Normal Cases

Adequate visualization of the anatomic morphology of the cauda equina nerve bundles (Figs. 1–3) was achieved in most of our cases (Table 1).

Anatomically, the nerve roots of the cauda equina descend alongside the conus medullaris and are densely packed into bundles located ventrolateral and dorsolateral (right and left) to the conus [11] (Figs. 1B and 2B). The conus is fairly distinguishable from the cauda equina nerve root bundles on the axial as well as on the sagittal sections (Figs. 1A and 2A). In the median sagittal slice (Fig. 1A), the conus is usually longer and more pointed than in the off-midline section, observed in 11 (79%) of the 14 volunteers we studied. Below the conus the nerve roots are predominately situated in the posterior part of the dural sac and they become more diffusely spread within the subarachnoid space (Figs. 2C and 2D).

In sagittal sections, they together appear as a uniform structure (Figs. 1A and 1C). However, the individual nerve roots become visible as they descend anteriorly and laterally toward their exits (Fig. 3A) under the pedicles. At this point they invariably appear thin (less than 2 mm in diameter as measured on the monitor using a cursor), smooth, and linear. On the sagittal image at the pedicular level, the nerve-root-sleeve unit is clearly shown in the upper part of the neural foramen contrasted by the surrounding fat (Fig. 3C). In addition to the nerve-root unit, multiple veins (usually numbering between two and five) are visualized within the intervertebral foramen, located both in the upper and lower part of the foramen (Figs. 3C, 3D, and 8). These veins traverse the foramen and interconnect with the internal vertebral and paravertebral venous plexuses. Coronal sections provided an excellent view of the anatomy of the nerve roots within the intervertebral foramina (Fig. 8). Occasionally, on T2-weighted sagittal images, a low-intensity longitudinal line was seen (Table 1 and Fig. 4), which did not correlate with any anatomic structure. This false finding may be attributed to the CSF pulsation [12].

Pathologic Cases

Alteration in the morphology of the cauda equina was observed in all three patients (Figs. 5–7). In case 1, the lesion at surgery was seen as multinodular masses adherent to the nerve roots in the upper lumbar region. The morphology of the lesion correlated closely with that seen on the T2-weighted MR images, more correctly than with the T1-weighted images (Fig. 5).

In case 2, surgical exploration revealed nodular masses involving the conus medullaris, the cauda equina nerve roots, and the thecal cul de sac, correlating with the findings on the MR images (Figs. 6B and 6C). On T1-weighted images, the lesions were indistinguishable from the surrounding CSF (Fig.

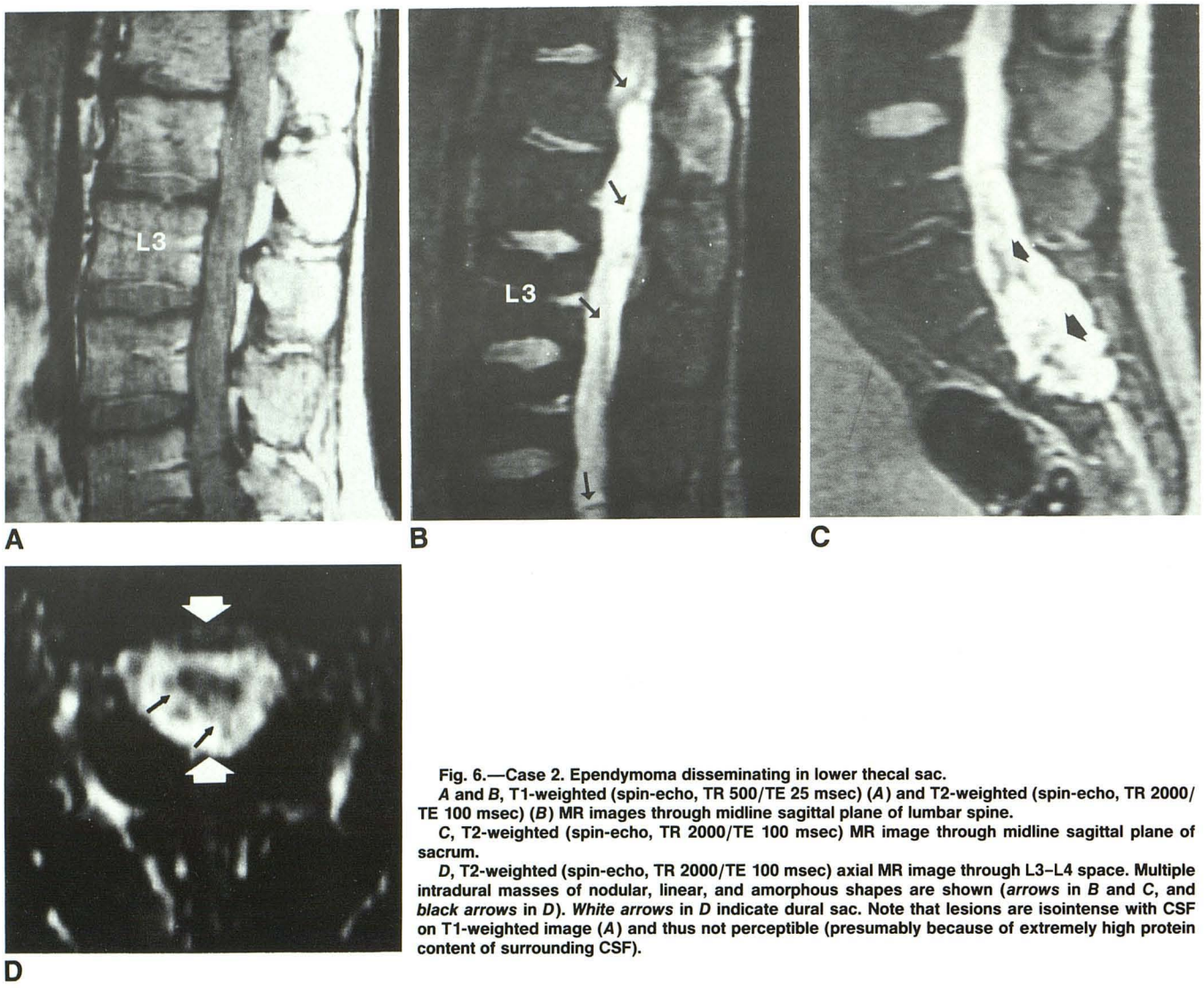

Fig. 6.—Case 2. Ependymoma disseminating in lower thecal sac.

***A* and *B*, T1-weighted (spin-echo, TR 500/TE 25 msec) (*A*) and T2-weighted (spin-echo, TR 2000/TE 100 msec) (*B*) MR images through midline sagittal plane of lumbar spine.**

***C*, T2-weighted (spin-echo, TR 2000/TE 100 msec) MR image through midline sagittal plane of sacrum.**

***D*, T2-weighted (spin-echo, TR 2000/TE 100 msec) axial MR image through L3–L4 space. Multiple intradural masses of nodular, linear, and amorphous shapes are shown (*arrows* in *B* and *C*, and *black arrows* in *D*). *White arrows* in *D* indicate dural sac. Note that lesions are isointense with CSF on T1-weighted image (*A*) and thus not perceptible (presumably because of extremely high protein content of surrounding CSF).**

6A). Lumbar puncture in this patient revealed viscous CSF with a protein concentration about 100 times higher than normal. The extremely high protein content could theoretically have shortened the T1 value of the CSF, consequently lowering its contrast differentiation with the tumor masses.

The tumors in cases 1 and 2 were ependymomas of the myxopapilloma type [13]. This tumor arises almost always from the filum terminale and frequently (75% of the instances) infiltrates the cauda equina nerve roots and/or the conus medullaris. It may sometimes disseminate in the subarachnoid space, but is usually limited to the lumbosacral thecal sac [14].

The metastatic melanoma tumors (case 3) exhibited a high signal intensity and were clearly seen as multiple nodules along the nerve root bundles (Fig. 7A). The lesions were imperceptible on the T2-weighted pulse sequence image as they become isointense with the high-intensity CSF (Fig. 7B).

Conclusions

MR proved efficient in defining the anatomy of the cauda equina. Morphologic alterations due to tumors infiltrating the nerve roots were correctly perceived while both T1- and T2-weighted pulse sequence imaging was used.

ACKNOWLEDGMENTS

We thank Joan Tudisco for secretarial assistance and Ronald J. Paris for photographic assistance.

REFERENCES

1. Han JS, Kaufman B, El Yousef S, et al. NMR imaging of the spine. *AJR* **1983**;141:1137–1145, *AJNR* **1983**;4:1151–1159
2. Modic MT, Weinstein MA. Pavlicek W, et al. Nuclear magnetic resonance of the spine. *Radiology* **1983**;148:757–762

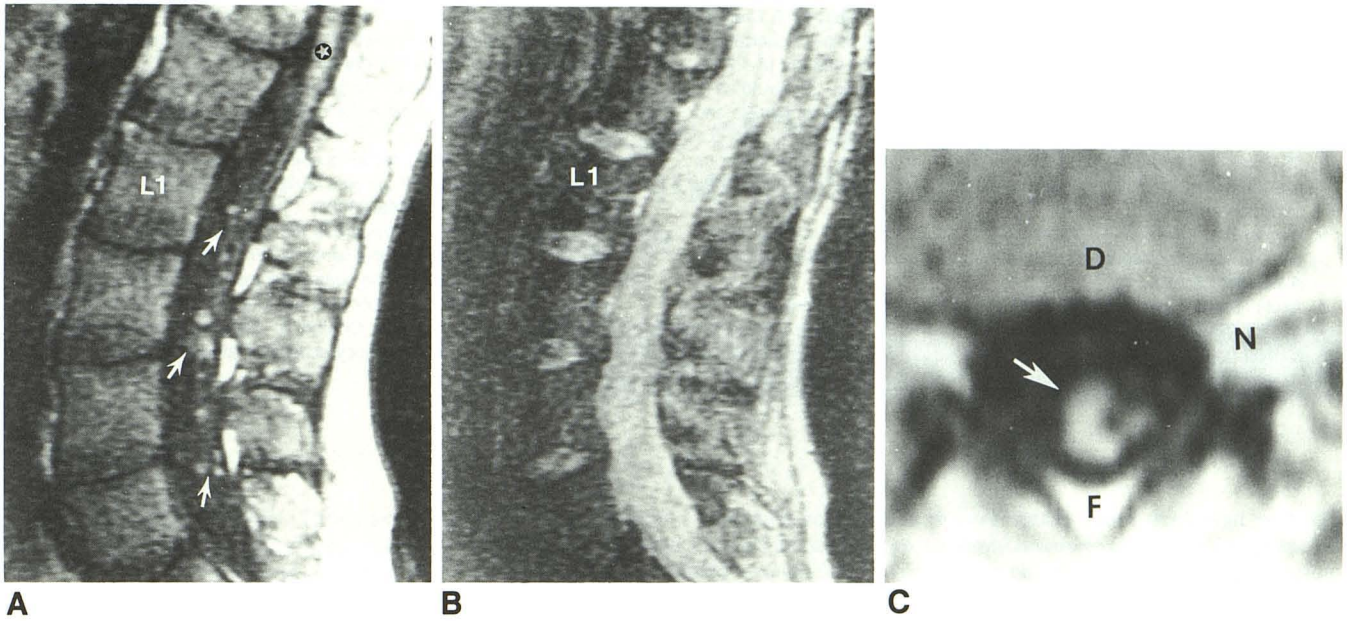

Fig. 7.—Case 3. Melanoma seeding to cauda equina nerve roots.

A and *B*, T1-weighted (spin-echo, TR 500/TE 25 msec) (*A*) and T2-weighted (spin-echo, TR 2000/TE 100 msec) (*B*) MR images through midline sagittal plane of lumbar spine.

C, T1-weighted (spin-echo TR 500/TE 25 msec) axial MR image through L3–L4 space. High-intensity nodular masses along nerve root bundles of cauda equina are clearly shown (*arrows* in *A* and *C*). The conus is indicated by *asterisk*. Note that lesions are isointense with high-intensity CSF on T2-weighted image (*B*) and thus not perceptible. *D* = intervertebral disk; N = neural foramen; f = epidural fat.

Fig. 8.—Coronal view of conus medullaris, cauda equina, nerve roots, and intervertebral foramen.

A, T1-weighted (TR 500 /TE 25 msec) coronal MR image through intervertebral foramen at thoracic-lumbar region. (Anterior to posterior aspect of spinal canal of normal volunteer was sectioned using 3-mm-thick contiguous slices, spin-echo sequence, TR 500/TE 25 msec, 256 × 256 matrix, 20-cm field of view, pixel size 0.78 × 0.78 mm, and six excitations. An axial localizing image was used for section localization.)

B, Matching anatomic section from undistorted cadaver specimen. The conus (*asterisk*), cauda equina, and nerve roots (*arrows*) are nicely demonstrated by MR. The contents of intervertebral foramen fat (f), nerve root (*large arrows*), ganglion (G), and veins (V) are shown. Note proximity of nerve roots to medial and inferior aspect of pedicle (P). Also note their steep course both inside dural sac (*small arrows*) and within foramen (*large arrows*). Their typical location and orientation within foramen help to identify them easily. Dorsal root ganglion lies at outlet of foramen. P1 and P2 = L1 pedicle and L2 pedicle. Anterior median fissure within cord (*black arrowheads*) should not be mistaken for central canal of spinal cord. In lower spine, the fissure enters deep into cord (Fig. 1B); consequently, a coronal section through anterior portion of cord (such as the section above) will cross the anterior median fissure.

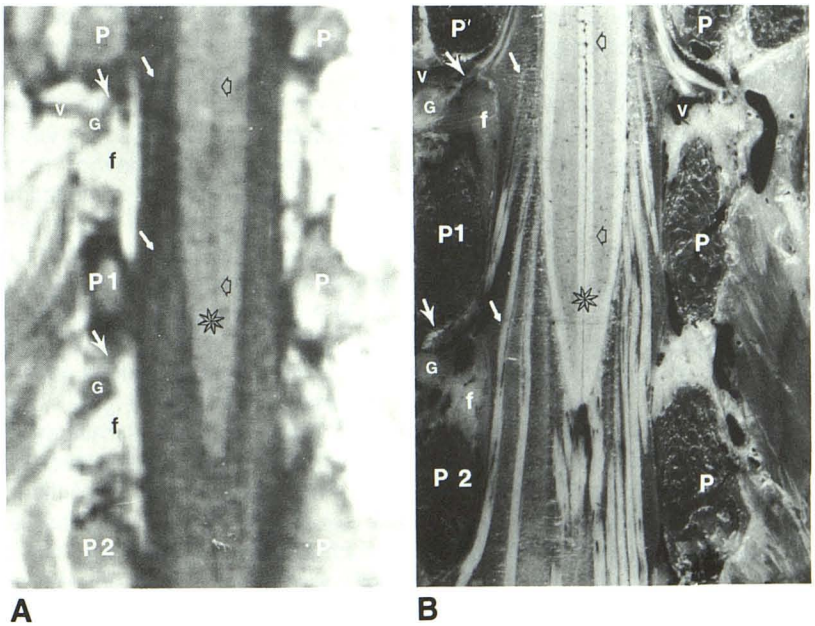

3. Modic MT, Weinstein MA, Pavlicek W, Boumphrey F, Starnes D, Duchesneau PM. Magnetic resonance imaging of the cervical spine: technical and clinical observations. *AJR* **1983**;141:1129–1136, *AJNR* **1984**;5:15–22
4. Norman D, Mills CM, Brant-Zawadzki M, Yeats A, Crooks LE, Kaufman L. Magnetic resonance imaging of the spinal cord and canal: potentials and limitations. *AJNR* **1983**;141:1147–1152
5. Di Chiro G, Doppman JL, Dwyer AJ, et al. Tumors and arteriovenous malformations of the spinal cord: assessment using MR. *Radiology* **1985**;156:689–697
6. Hyman RA, Edwards JH, Vacirca SJ, Stein HL. 0.6 MR imaging of the cervical spine: multislice and multiecho techniques. *AJR* **1985**;6:229–236, *AJNR* **1985**;6:229–236
7. Axel L. Surface coil magnetic resonance imaging. *J Comput Assist Tomogr* **1984**;8:381–384
8. Bilaniuk LT, Zimmerman RA, Wehrli FW, et al. Cerebral magnetic resonance: comparison of high and low field strength imaging. *Radiology* **1984**;153:409–414
9. Schenck JF, Foster TH, Henkes JL, et al. High-field surface-coil MR imaging of localized anatomy. *AJNR* **1985**;6:181–186
10. Rauschning W. Computed tomography and cryomicrotomy of lumbar spine specimens: a new technique for multiplanar anatomic correlation. *Spine* **1983**;8(2)170–180
11. Rauschning W. Detailed sectional anatomy of the spine. In: Stephen LG, Rothman MD, Glenn WV Jr, eds. *Multiplanar CT of the spine.* Baltimore: University Park Press, **1985**:33–85
12. Sherman JL, Citrin CM, Gangarosa RE, Bowen BJ. The MR appearance of CSF pulsations in the spinal canal. *AJNR* **1986**;7:879–884
13. Rubinstein LJ. Tumors of the central nervous system. In: *Atlas of tumor pathology*. Maryland: Armed Forces Institute of Pathology, **1979**:118–119
14. Sonneland PR, Bernd WS, Onofrio B. Myxopapillary ependymoma: a clinicopathologic and immunocytochemical study of 77 cases. *Cancer* **1985**;56:883–893